EPJ Web of Conferences **17**, 03006 (2011)
DOI: 10.1051/epjconf/20111703006

Study of reactions with the weakly bound projectile ^{9}Be with ^{89}Y

C.S. Palshetkar[1,a], S. Santra[1], A. Chatterjee[1], K. Ramachandran[1] Shital Thakur[2], S.K. Pandit[1], K. Mahata[1], A. Shrivastava[1], V.V. Parkar[3], V. Nanal[2], B.J. Roy[1], V. Jha[1] and, and S. Kalias[1]

[1] Nuclear Physics Division, Bhabha Atomic Research Centre, Mumbai- 400 085, India
[2] Department of Nuclear and Atomic Physics, Tata Institute of Fundamental Research, Mumbai- 400 005, India
[3] Departamento de Física Aplicada, Universidad de Huelva, E-21071 Huelva, Spain

Abstract. With the aim to investigate the influence of the breakup channel on different reaction channels, the elastic scattering and fusion of ^{9}Be with the medium mass target ^{89}Y has been studied at near barrier energies. Optical model analysis of the elastic data has been carried out and a dispersion relation applied to the real and imaginary potentials to investigate their energy dependence from which the presence of breakup threshold anomaly has been observed. Complete fusion (CF) cross sections, obtained for ^{9}Be+^{89}Y system, are found to be suppressed by (20 ± 5)% as compared to the coupled-channels calculations without breakup coupling. This observation has been further confirmed by comparing these cross sections with those for the ^{4}He+^{93}Nb and ^{12}C+^{89}Y systems, where fusion is induced by a tightly bound projectile and forms a nearby compound nucleus to that formed by ^{9}Be+^{89}Y. Results from the breakup coupling done in continuum discretized coupled-channels calculations show that the elastic cross sections thus obtained, which also fit the experimental elastic cross sections, are enhanced compared to the uncoupled calculations which implies a reduction in absorption/fusion cross sections. These enhanced cross sections suggest that the dynamic polarization potential produced due to breakup coupling is repulsive in nature. Thus the effective (bare+polarization) potential around the barrier becomes less attractive leading to the absence of the normal threshold anomaly.

1 Introduction

Reactions induced by weakly bound projectiles have been rigorously studied over the last two decades. Interest in the field developed due to their importance in understanding the nucleosynthesis process and studying nuclei near the drip lines. Due to the low breakup threshold for these nuclei, the effect of the breakup channel on other reaction channels is expected to be important. Two main types of investigations have been carried out to study this effect: (i)Optical model analysis (OMA) of elastic scattering data, where the energy dependence of the real and imaginary potentials is observed and (ii)Analysis of the fusion data, where comparison of the CF cross sections with the coupled-channels (CC) calculations is done.

From the OMA of the elastic scattering data for the weakly bound stable nuclei, the breakup threshold anomaly (BTA) has been observed, where the imaginary potential persists even at below barrier energies (increases at below barrier energies before reducing to zero) while the real part in the same energy region shows a slight reduction. This, however, is opposite to the usual threshold anomaly (TA), observed in the case of OMA of the elastic data for the tightly bound projectiles, where the imaginary part is nearly constant above the barrier and decreases to zero below the barrier while the real part shows the bell shaped maximum around the barrier. The observation of BTA has been explained in terms of a repulsive dynamic polarization potential (DPP) generated due to breakup coupling, which compensates the attractive polarization arising due to coupling to bound states [1]. In the case of the weakly bound stable nuclei, the BTA has been observed for elastic scattering of ^{6}Li from different mass targets while the TA has been observed for ^{7}Li scattering [2]. For similar measurements carried out using ^{9}Be projectile, no TA has been observed for ^{9}Be+^{27}Al [3], ^{9}Be+^{144}Sm [4], inconclusive results for ^{9}Be+^{12}C [5], ^{9}Be+^{64}Zn [6] and ^{9}Be+^{209}Bi [7], while the TA has been observed for the ^{9}Be+^{208}Pb system [8].

In the case of fusion of the weakly bound stable nuclei, a suppression of the CF cross sections has been observed at above barrier energies as compared to the CC calculations without inclusion of breakup coupling. Particularly, for fusion reactions induced by ^{9}Be projectile, a suppression of ∼32% of CF cross sections for the ^{9}Be+^{208}Pb [9] and ^{9}Be+^{209}Bi [10] has been observed. For fusion with light mass targets, only the total fusion (TF) i.e, CF + incomplete fusion (ICF) (where only one of the fragment of the projectile af-

[a] e-mail: chandani@barc.gov.in

ter breakup fuses with the target) could be measured for the ^{9}Be+^{27}Al [11] and ^{9}Be+^{64}Zn [12,13] systems. Comparison of these experimental fusion cross sections with CC calculations does not show any suppression [12]. The supression of CF cross sections observed in case of fusion with heavy targets is suggested to be due to loss of flux from the CF channel due to breakup of the projectile in the field of the target thus leading to ICF [9].

Thus with the aim to study the influence of breakup channel on the scattering and fusion of the weakly bound nucleus ^{9}Be with a medium mass target at near barrier energies, we have carried out the elastic scattering and fusion measurements for the ^{9}Be+^{89}Y system.

2 Elastic scattering of ^{9}Be from ^{89}Y

The measurement was carried out at the 14UD Pelletron-Linac facility at Mumbai, India, inside a 1 m diameter scattering chamber having two rotatable arms. Silicon surface barrier detectors (SSBs) in the ΔE-E telescopic configuration, with thicknesses between 25-33 μm and 0.5-1 mm respectively, were mounted on one arm to detect the elastically scattered ^{9}Be particles. Another SSB, mounted on the other arm at a forward angle of 25^{o} with respect to the target, was used as a monitor. Angular distribution ($25^{o} \leq \theta_{lab} \leq 175^{o}$) of the scattered ^{9}Be particles from ^{89}Y target ($\sim$650 μm thick) were obtained for ^{9}Be beam (current 5-15 nA) energies from 19 to 33.5 MeV in steps of 2 MeV.

The ratio of the experimental elastic to the Rutherford cross sections as a function of center-of-mass angle of the scattered ^{9}Be particles is shown in Fig. 1 by unfilled circles.

Optical model analysis for the system has been carried out using the code FRESCO [14]. The optical model potential of the form U(r)=V_c(r)-λV(r)-iW(r) was used in the calculations where V_c(r) is the Coulomb potential, V(r) the real part of the nuclear potential taken to be of the microscopic double folding type, λ is the normalization constant for V(r) and W(r) is the imaginary part of the nuclear potential taken to be of the Woods-Saxon form. The double folding potential was calculated using the code DFPOT [15], were the nuclear charge distributions for ^{9}Be and ^{89}Y have been taken from Ref. [16] and Ref. [17] respectively. Initial calculations were carried out with λ=1, W_o=20 MeV, a_w=0.65 fm. The search version SFRESCO was then employed to get the best fit parameters for λ, W_o and a_w keeping r_w=1.22 fm fixed. The results from the best fit parameters are shown in Fig. 1 by solid lines. The energy dependence of the real and imaginary potentials has been represented by plotting them at the strong absorption radius (R_{sa}=10.5 fm for the system) as a function of the center-of-mass energy of ^{9}Be as shown in Fig. 2. A dispersion relation has been applied to get the theoretical predictions for the real part of the potential from

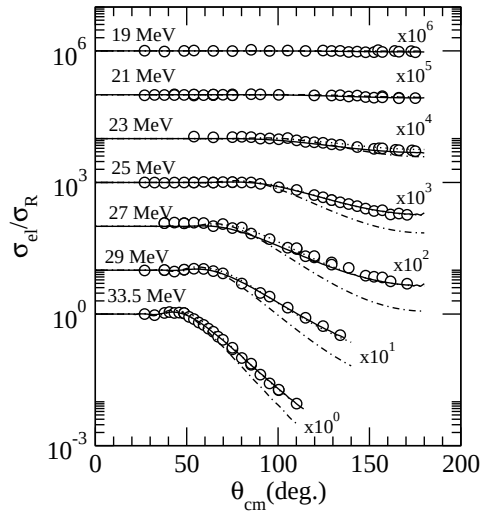

Fig. 1. Ratio of the elastic scattering cross sections to the corresponding Rutherford values as a function of center-of-mass angle of the elastically scattered ^{9}Be at different beam energies. The solid lines are the results from OMA. The dot-dash lines are results for the uncoupled calculations and the dotted lines (overlapping with the solid line in fig.) represent results after continuum breakup coupling.

the imaginary potential using the best fit parameters obtained from the optical model analysis. The results thus obtained are shown in Fig. 2 as the solid line. The dotted and the dashed line represents two other possible segments for the imaginary potential considered to obtain the real part using the dispersion relation.

Continuum distretized coupled channels (CDCC) calculations have been carried out for the system, to study the effect of breakup on the elastic channel, using the code FRESCO. In the present calculations ^{9}Be has been taken to have a cluster structure of ^{5}He(core)+^{4}He(valence) [18]. The binding potential for the cluster has been taken from [19]. Woods Saxon form for the ^{4}He+^{89}Y and ^{5}He+^{89}Y potentials was considered, with the diffuseness for the latter incremented by 0.1 fm as compared to the former. The initial values for the ^{4}He+^{89}Y potential were taken from [20]. Coupling to the $5/2^{-}$ (E=2.42 MeV) and $7/2^{-}$ (E=6.38 MeV) excited states in ^{9}Be has also been included by considering them as pure L=2 states. Though the ^{9}Be $\rightarrow 2\alpha$+n breakup threshold energy is 1.57 MeV thus implying that $5/2^{-}$ and $7/2^{-}$ are unbound states, however since in the present calculations ^{9}Be is assumed to breakup dominantly into ^{5}He+^{4}He (having threshold energy 2.467 MeV) the $5/2^{-}$ state has been taken as a bound excited state and $7/2^{-}$ a resonant state with ΔE=3.0 MeV width energy bin centered at resonance energy 6.38 MeV. Again the same binding potential as that used for the ground state has been used for these states with the depth being adjusted to give the correct binding energy. Along with these excited states, a ^{5}He+^{4}He continuum has been included in the calculations by discretizing it between $0.52 \leq k \leq 0.82$ fm^{-1} with bin of Δk=0.15 fm^{-1}.

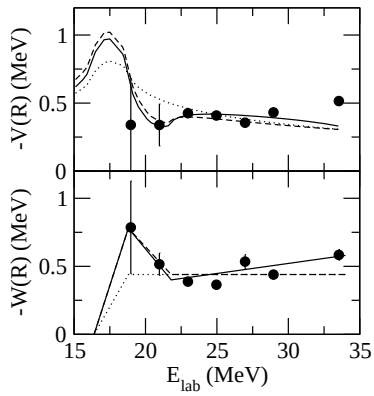

Fig. 2. Real and Imaginary potentials plotted at the strong absorption radius as a function of the center-of-mass energy of ^{9}Be beam. The solid line represents the theoretical predictions for the real part (a) after inputting the imaginary part using the segments as shown in (b). The dotted and dashed lines represents two other possible segments considered for the imaginary part.

The L=0,1,2 continuum has been used in the calculations. Again binding potential of Woods-Saxon form for the continuum state has been taken, same as that for the ground state. Re-orientation coupling for the ground state of ^{9}Be has been included in the calculations since it is highly deformed with $\beta \sim 1.3$. The results from the CDCC calculations are shown in Fig. 1 by dotted lines.

A recent exclusive breakup measurement [21] shows that the α observed at sub-barrier energies with a broad continuum are predominantly from the prompt breakup of ^{9}Be. It is suggested that this prompt component can affect fusion leading to ICF and thus the observed suppression in CF cross sections [22]. To find out what fraction does the breakup cross section form of the reaction cross section, inclusive breakup α cross sections have been extracted from the α band obtained in the elastic scattering data of ^{9}Be+^{89}Y. From kinematics, the minimum and maximum α energies between which breakup events can be obtained have been calculated and the α yields have then been extracted between these energy limits. (Contamination to the α yield can also arise from α evaporated from the compound nucleus (CN). However, statistical model calculations show this contribution to be negligible). These cross sections were further integrated to get the total inclusive breakup α cross sections plotted in Fig. 3 by unfilled diamonds, along with the reaction cross sections obtained from the optical model analysis of the elastic data (filled circles) and CF cross sections (filled triangles) obtained from a separate measurement carried out by us (as detailed below).

3 Fusion of ^{9}Be with ^{89}Y

The measurement was carried out at the 14UD Pelletron-Linac facility at Mumbai, India. Offline γ-counting

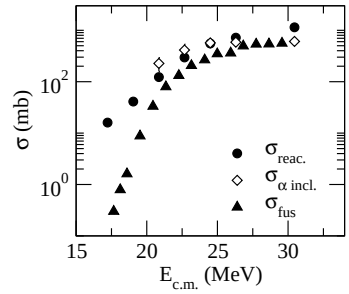

Fig. 3. Reaction (circles), inclusive breakup α (diamonds) and CF (triangles) cross sections for the ^{9}Be+^{89}Y system.

method was used for the investigation. A HPGe detector was used for detecting the γ coming from the evaporation residues (ERs) after particle evaporation from the compound nucleus (CN). ^{89}Y targets ($\sim$0.93 mg/cm^2 thick) were irradiated with ^{9}Be beam at energies from 20 to 33 MeV in steps of 1 MeV. Aluminum catcher foils ($\sim$1 mg/cm^2 thick) were used along with the ^{89}Y target foils to stop the recoiling ERs. The beam current during each irradiation was monitored by recording the total integrated current in intervals of 1 min using a CAMAC scaler. Energy calibration and efficiency of the detector were obtained using standard ^{152}Eu and ^{133}Ba sources.

Two other fusion measurements, in which a tightly bound projectile fuses with the target to give same or nearby compound nucleus to the one formed by fusion of ^{9}Be+^{89}Y (i.e ^{98}Tc), were also carried out. The ^{4}He+^{93}Nb (CN- ^{97}Tc) and ^{12}C+^{89}Y (CN- ^{101}Rh) systems were chosen for the measurements. The experimental setup for these two measurements is the same as that for ^{9}Be+^{89}Y, details of which are given in Ref. [24].

Fusion of ^{9}Be with ^{89}Y forms the CN ^{98}Tc in an excited state which then cools down mainly via particle evaporation. The 2n, 3n, 4n and α2n evaporation channels as well as the 1n transfer channel, were observed (identified from their characteristic γ-lines) in the offline counting. Out of these the 2n and 3n evaporation channels were found to be dominant($\sim$ 80-90% of σ_{fus} as estimated from the statistical model code PACE [25]) over the entire energy range studied. The unaccounted 10-20% of cross sections due to formation of stable ERs were taken into account from PACE by taking the ratio R= $\Sigma_x \sigma_{xn}^{PACE}/\sigma_{fus}^{PACE}$ where x=2,3,4 and using this ratio to calculate the CF cross sections by σ_{fus}^{expt}=$\Sigma_x \sigma_{xn}^{expt}$/R [24] plotted in Fig. 3 by filled triangles. A lower limit of the ICF cross sections due to partial fusion of α with ^{89}Y was also estimated [24]. CC calculations using the code CCFULL [26] were done in which coupling to the projectile and target excited states was done as well as effect of projectile ground state spin was considered. The results from the CC calculations have been plotted as the dotted line in Fig. 4a and b. A comparison of experimental CF cross sections for the ^{9}Be+^{89}Y system was done with the fusion cross sections for the ^{4}He+^{93}Nb and ^{12}C+^{89}Y

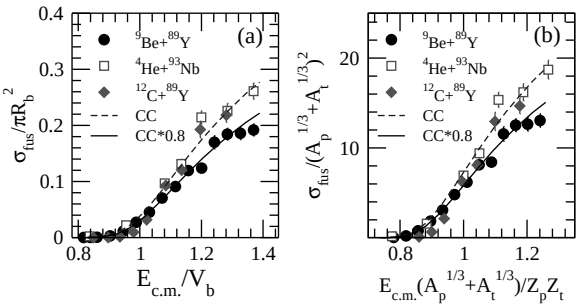

Fig. 4. Reduced experimental fusion cross sections for the ^{9}Be+^{89}Y system (filled circles) along with the corresponding values for the ^{4}He+^{93}Nb and ^{12}C+^{89}Y systems.

system and are plotted in Fig. 4. Two reduction procedures have been used for making the comparison. In the first method, $\sigma_{fus}/\pi R_b^2$ versus E_{cm}/V_b has been plotted as shown in Fig. 4a. In the second method the geometrical dependence has been eliminated in an approximate way by taking $R_b=r_o(A_p^{1/3}+A_t^{1/3})$ and $V_b=Z_pZ_te^2/R_b$ [27] shown in Fig. 4b. V_b for the ^{9}Be+^{89}Y system has been extracted from the barrier distribution following the procedure given in [28] while that for ^{4}He+^{93}Nb and ^{12}C+^{89}Y systems has been obtained from the default Woods-Saxon parametrization of the Akyuz-Winther potential.

4 Results and Conclusions

The dispersion relation is satisfied by the ^{9}Be+^{89}Y system. From Fig. 2 it can be seen that the imaginary potential persists, increases at below barrier energies. This observation is as opposed to the conventional TA where it is found to decrease with decreasing energy below the barrier. This suggests that the usual TA is absent for the ^{9}Be+^{89}Y system. Inclusion of the continuum breakup coupling shows that the elastic cross sections thus calculated (dotted line in Fig. 1), and which also fit the experimental elastic cross sections, are enhanced at backward angles as compared to the uncoupled ones (dot-dash line in Fig. 1). This suggests that the DPP produced due to coupling to breakup states is repulsive in nature which explains the observed BTA for the system. From Fig. 3 it can be seen that the inclusive breakup α cross sections form a large part of the reaction cross sections over the entire energy range. Especially at below barrier energies the two are nearly equal thus suggesting that breakup channel is indeed the dominant reaction channel for the system.

Comparison of CF cross sections for the system with the CC calculations, which do not include the effect of breakup coupling, show that the former are suppressed by $(20 \pm 5)\%$ compared to the latter, especially at above barrier energies. The enhanced elastic cross sections obtained from breakup coupling at backward angles implies a reduction in the absorption/fusion cross sections. Thus the suppression of CF cross sections observed at above barrier energies can be explained to be due to the repulsive DPP for the system thus leading to reduced absorption. Comparison of the CF cross sections for the system with those for ^{4}He+^{89}Y and ^{12}C+^{89}Y system further confirms the 20% suppression observed for the ^{9}Be+^{89}Y system. If the breakup channel would not have been affecting the fusion channel, the cross sections for the three systems would have matched since the three systems form nearby CN. Thus, the difference in the cross sections observed can be attributed to the weakly bound nature of the ^{9}Be projectile.

References

1. N. Keeley et al., Nucl. Phys. **A571**, (1994) 326
2. L.F. Canto et al., Phys Rep. **424**, (2006) 1 and references therein.
3. P.R.S. Gomes et al., Phys. Rev. C **70**, (2004) 054605.
4. A. Gómez Camacho et al., Phys. Rev. C **77**, (2008) 054606
5. A.T. Rudchik et al., Nucl. Phys. A **662**, (2000) 44
6. S.B. Moraes et al., Phys. Rev. C **61**, (2000) 064608; P.R.S. Gomes et al., Phys. Rev. C **71**, (2005) 034608
7. C. Signorini et al., Phys. Rev. C **61**, (2000) 061603(R)
8. R. J. Woolliscroft er al., Phys. Rev. C **69**, (2004) 044612
9. M. Dasgupta et al., Phys. Rev. Lett. **82**, (1999)1395
10. M. Dasgupta et al., Phys. Rev. C **81**, (2010) 024608
11. R.M. Anjos et al., Phys. Lett. B **534**, (2002) 45; G.V. Martí et al., Phys. Rev. C **71**, (2005) 027602
12. P.R.S. Gomes et al., Phys. Lett. B **601**, (2004) 20;
13. P.R.S. Gomes et al., Phys. Rev. C **71**, (2005) 034608
14. I.J. Thompson, Fresco (May 2007), version FRES 2.3
15. J. Cook, Comp. Phys. Commun. 25, (1982) 125
16. V. Hnizdo et al., Phys. Rev. C **24**, (1981) 1495
17. H.D. Vries et al., At. Data Nucl. Data Tables **36**, (1987) 495
18. K. Arai et al., Phys. Rev. C **54**, (1996) 132
19. N Keeley et al., Phys. Rev. C **64**, (2001) 031602(R)
20. M. Nolte et al., Phys. Rev. C **36**, (1987) 1312
21. R. Rafiei et al., Phys. Rev. C **81**, (2010) 024601
22. D. Hinde et al., Phys. Rev. Lett. **89**, (2002) 272701
23. G.G. Kiss et al., Phys. Rev. C **80**, (2009) 045807
24. C.S. Palshetkar et al., Phys. Rev. C **82**, (2010) 044608
25. A. Gavron, Phys. Rev. C **21**, (1980) 230
26. K. Hagino et al., Comp. Phys. Commun. **123**, (1999) 143
27. P.R.S. Gomes et al., Phys. Rev. C **71**, (2005) 017601
28. M. Dasgupta et al., Annu. Rev. Nucl. Part. Sci. **48**, (1998) 401